Analysis of propeller slipstream effects on a trailing wing

L.L.M. Veldhuis
Low Speed Aerodynamics Laboratory
Delft University of Technology
Kluyverweg 1, 2629 HS Delft, the Netherlands

Abstract A low aspect ratio semi-span wing model combined with a 4 bladed tractor propeller was tested in the Delft University Low Speed Windtunnel. To enable investigation of the propeller position effects the nacelle could be disconnected from the wing. Based on external balance measurements and surface pressure measurements for both configurations with propeller on and off the effects of the propeller slipstream on the overall aerodynamic coefficients were determined. Besides fundamental information about the interaction effects between the propeller and the wing the experimental results reveal that substantial performance benefits can be obtained. In this respect the propeller angle of attack seems to have a dominant influence on the wing performance. Mounting the propeller at a negative (tilt down) angle with reference to the wing suggests a strong reduction of overall wing induced drag. Besides this, the wing efficiency is found to be strongly dependent on both the spanwise and vertical position of the propeller. A flow field survey performed with a 5-hole pressure probe at 1 chord length behind the model reveals important qualitative and quantitative information on the propeller dominated interactive flow.

Symbols

b	wing span
c	wing chord
C_D	drag coefficient
C_L	lift coefficient
C_l	local lift coefficient
C_n	local normal force coefficient
C_p	static pressure coefficient
C_{p_t}	total pressure coefficient $(= (P_t - P_{t_\infty})/q_\infty)$
C_t	local tangential force coefficient
D	propeller diameter, drag force
e	Oswald efficiency factor
H	total pressure
J	advance ratio $(= V/nD)$
L	lift force
n	propeller speed (Hz)
P_c	power coefficient $(= P/\rho V^3 D^2)$
q	dynamic pressure
R	propeller radius
Re	Reynolds number based on the m.a.c.
T_c	thrust coefficient $(= T/\rho V^2 D^2)$
S	wing area
U_e	effective velocity
u, v, w	components of the flow velocity vector
u^*	Betz' velocity
u_b	blockage velocity according Maskell
x_p, y_p, z_p	propeller position (center of spinner in propeller plane)
α	wing angle of attack
α_p	propeller angle of attack
δ_{fi}, δ_{fo}	inboard, outboard flap deflection
ΔP_t	total pressure jump across the propeller plane
η_{eff}	effective efficiency
ξ	axial vorticity $= (\partial w/\partial y - \partial v/\partial z)$
ρ	air density
ϕ	scalar function
ψ	scalar function

Indices

$1, 2$	at survey planes 1 and 2 respectively
l	lower windtunnel wall
p	of the propeller
u	upper windtunnel wall
v	vortex component
w	of the wing
∞	at infinity

Introduction

Since modern turboprop aircraft tend to have higher disk loadings the aerodynamic behaviour of propeller powered aircraft has become more complex. First there are the direct effects of forces and moments acting on the propeller while secondly the increased energy in the slipstream causes stronger interference effects on other aircraft parts than previously encountered. This has accentuated the need to optimize the integration of the propulsion system in connection with the reciprocal influence of the propeller slipstream on other aircraft components. In this field different aspect play an important

role like : aerodynamic performance, stability and control, structural loading and noise production. During the last decade several innovations like utilization of : blade sweep, advanced blade airfoil sections, counter-rotation and spinner area ruling have increased the fuel efficiency of the propeller. Generally however, the propeller is active in a flow field where strong interactions with its supporting structure, like a wing, play a role. Consequently, the combined performance of the propeller plus other aircraft parts should be examined. One important aspect when looking at the performance effects is the fact that a considerable part of the power absorbed by the propeller is wasted through the generation of swirl, which does not contribute to the thrust. To overcome this problem propulsion systems with contra-rotating propellers have been developed to recover most of the swirl. They are however not extensively used because of their complexity and weight. Since the swirl velocity affects the lift distribution of a trailing wing it is clear that the induced drag is influenced directly. In this respect, analyses by Kroo [1] , Miranda & Brennan [2] and Veldhuis [6] have indicated that significant wing drag reduction can be obtained for propeller/wing interaction.

Rather than manipulate wing geometry to approach two-dimensional flow, it would seem logical to use some energy source for the task of directing the flow such that lower wing induced drag is produced. As will be shown furtheron, the rotational component in the slipstream, which has always been considered to represent lost energy, is in fact available for amplifying or attenuating the wing vortex system with a possible reduction of induced drag. When examining the problem in detail it is found that several options are available for enhancing the performance of propeller/wing configurations. As shown by Takallu & Gentry [7] the lift coefficient of a powered wing with deployed high lift devices could be increased by the propeller slipstream. They also found that a pitch down nacelle inclination and vertical placement are important parameters for optimizing the aerodynamic performance of high lift transport aircraft with highly loaded propellers. However, contrary to the results discussed hereafter, the lift augmentation found during their investigation was always associated with an additional increase in drag.

To explore further the aerodynamic phenomena which play a role in this process and to derive a better fundamental understanding of the interactive flows causing slipstream / wing interference, a research program based on theoretical as well as experimental methods was set up at the Low Speed Aerodynamics Laboratory of Delft University of Technology. The results will be used to validate design codes and propeller / wing calculation models currently under development. The final objective is to define optimum low speed tractor propeller/wing configurations. The present work comprises an experimental effort that adresses the mutual influence between a propeller and a low aspect ratio wing. The aim of this paper is to present some results of experimental investigations that were performed on a tractor propeller wing configuration and to show that performance benefits can indeed be obtained for tractor propeller/wing configurations. Besides this, a detailed flow field survey and surface pressure measurements provide qualitative as well as quantitative reference data to be used for validation of propeller/wing interference models.

Propeller/wing interaction effects

A tractor propeller placed in front of a wing induces regions of upwash and downwash on a part of this wing. The propeller induced upwash introduces an angle of attack increase, while the downwash side experiences a decreased angle of attack. With the wing at a positive angle of attack the wing generates a positive lift that results in an augmented lift at the upgoing blade side (UBS) and a decreased lift in the downwash region (DBS). Assuming an equal axial and tangential velocity increase on both sides the lift generated at the UBS will be higher than on the DBS, resulting in a net decrease of the wing induced drag. For finite wings the spanload gradients become important since a possibly higher lift at the UBS compared to the DBS, generally enhances the beneficial effect on induced drag. Thus for "elliptic-like" lift distributions, a propeller has the tendency to enhance drag reduction for inboard up rotation (IUR) and to diminish drag reduction for outboard up rotation (OUR).

The necessary conditions for wing drag reduction would therefore require the backward rotated force at the DBS to be smaller than the forward rotated force vector at the UBS. This means that wing tip mounted propeller configurations have maximum potency of drag reduction since the negative contribution of the downgoing blade side is removed completely. This was already indicated by Miranda & Brennan [2]. From the abovementioned, it becomes clear that any parametric variation which alters the wing's spanload distribution will affect the amount of swirl recovery and drag reduction. Not only the swirl velocities affect the wing's local angle of attack but also the slipstream contraction. This aspect becomes very important, as will be shown lateron, when the propeller and the wing are very close to each other.

Apart from the effect the propeller has on the wing, the velocities induced by the wing alters the propeller performance by modifying the local angles of attack on the blades. The upwash produced by the wing vortex system increases the angle of attack of the downgoing blade resulting in an augmented thrust and torque on the blade. The upgoing blade however experiences an angle of attack decrease and therefore the thrust and the torque are decreased on this blade.

The same effects occur when the propeller, without the wing present, is placed at a positive angle of attack. The

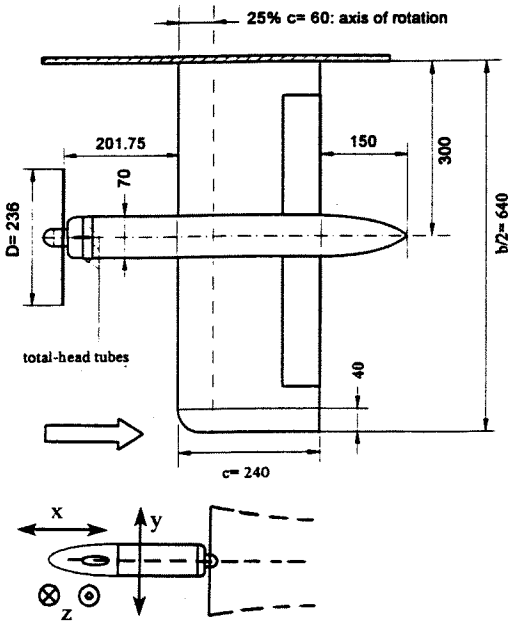

Figure 1: Layout of the windtunnel model(s). Dimensions in mm

way in which the propeller induced flow field is affected by the presence of the wing plays an important role for the possible drag reduction of the wing. This can be seen as follows. For a propeller, at positive angle of attack, a difference in swirl velocity at the wing position is found between the UBS and the DBS. As shown before a swirl distribution with lower values at the DBS and higher values at the UBS should result in more favorable characteristics e.g. an increase in the wing efficiency factor. The obvious way to accomplish this is the utilization of a larger negative propeller angle of attack (Veldhuis [6]). In this way two beneficial effects are combined. First the swirl distribution itself will become more favourable, secondly the whole slipstream will be placed at an angle of attack which attenuates the forward tilting process at both sides of the nacelle. Some results of this configuration with propeller tilt down angle, further referenced as the PTD-configuration, will be given in this paper.

Experiments

Experimental set-up

During the investigations two windtunnel models were used. The first one, called PROWIM (*PROpeller Wing Interference Model*) consists of a straight wing of aspect ratio 5.33 with no twist, and constant chord, equipped with a 4-bladed propeller. The axi-symmetrical nacelle was build as a "minimum body" mounted with its rotation axis on the MAC-line and 0.3m from the wing root (fig. 1). The symmetrical airfoil section used is *NACA 64-A015*. This allows investigation of both propeller inboard-up and outboard-up rotation by giving positive and negative angle of attack respectively. The wing is provided with 2 plain single slotted flaps located on both sides of the nacelle. Maximum deflection is limited to $\delta_f = \pm 40°$ by the tubing coming from the pressure taps in the flaps. The model was attached to the 6 component windtunnel balance through a turntable which is flush with the image plate situated at 0.3 m from the upper wall. The second model, further referenced as APROPOS (*Adaptive PROpeller POsitioning System*), is identical with the first but it is not provided with flaps and it has no nacelle connected to it. Instead the nacelle with propeller is supported by a strut which can be traversed with a 3 component traversing system with an accuracy of approximately 0.02 mm in all directions. For the APROPOS test the propeller could be set at positive or negative angle of attack with respect to the wing chord line.

To perform surface pressure measurements, the wing contains a total of 918 pressure taps located in 18 rows. In the viscinity of the nacelle, where the slipstream washes the wing, a closer spacing was used than outside this area. The surface pressure data were acquired using 2 scanivalves connected to 2 PCDR-22 pressure transducers installed on top of the test section. Two pitot tubes are installed at a small distance behind the propeller to determine the total pressure jump ΔP_t across the propeller plane. A linear relation between T_c and the dimensionless parameter $\Delta P_t/q$ exist which was used to indicate changes in the thrust coefficient during the measurements.

The propeller was driven by a 3-phase induction motor housed in the nacelle. Speed setting of this motor was controlled using a 200-per-revolution optical encoder mounted on the rotor. The torque (and power) delivered by the motor was measured by using an unique relationship between the current through the stator and the shaft torque output, found in earlier calibrations. Cooling of the motor was done through a closed cooling circuit filled with distilled water.

The test facility The windtunnel used during these investigations was the Delft University Low Turbulence Tunnel (LTT) which has an octagonal test section of $1.80 \times 1.25m$. A general description of this facility is given by Veldhuis [4]. Maximum speed is 120 m/s and the turbulence level ranges from 0.025% at 40 m/s to 0.085% at 100 m/s. A 6-component balance system (platform type) with automatic weigh beams of high accuracy is mounted above the test section.

To prevent loss of pressure data accuracy due to transducer drift the PCDR-22 pressure transducers, mounted outside the test section, were calibrated approximately every 10 minutes using an "on-line" calibration unit. During the 5 hole probe measurements the electronic pressure transducer (ZOC) was positioned inside the front part of the probe support and therefore sensitive to possible temperature changes. To compensate potential errors this transducer was therefore calibrated every 600

datapoints (approx. 3 minutes) using the same on-line calibration procedure.

Five hole probe and traversing mechanism To acquire velocity field data behind the wing, 5-hole probe measurements were performed. One of the purposes of these surveys was to explore the geometry of the deformed slipstream downwind of the wing for several settings of the model. The data were also used to calculate the lift, profile drag and induced drag of the model following a procedure similar to the one presented by Brune & Bogataj [5] and de Leeuw [11]. All test data were reduced on-line yielding the three components of wake velocity, from which circulation, kinetic energy and total pressure within the slipstream/wake were calculated. Traversing of the probe was done through a system consisting of a diffusor mounted x,y,z-slide and an adjustable sting connected to it.

The time needed for measuring several model configurations was minimized by reading the pressure transducer, while the probe was traversing at low speed ($5mm/s$). The DACU was triggered for measurement every 2 mm of y-movement using the signal output of an optical encoder connected to the y-shaft. The complete measurement cycle of one survey point took 24 ms. This means that the displacement effect ($0.024 \times 5 = 0.12mm$) of the traversing probe is negligible compared to the probe diameter.
Typically, the total measurement grid behind the model contains about 30,000 to 40,000 data points per flow case.

Test conditions Most of the measurements were conducted at a dynamic pressure of 1500 Pa ($Re = 0.8 * 10^6$). To increase the thrust coefficient of the propeller with limited available power of the model motor, for some conditions a lower value of 245 Pa ($Re = 0.3 \cdot 10^6$) was chosen. The complete set of test conditions is given in table 1.

Table 1: Test conditions

TEST	R_e	J	T_c
PROWIM	$0.8 \cdot 10^6$	$0.81 - 1.20$	$0.0 - 0.2$
APROPOS	$0.3 \cdot 10^6$	0.43	0.77
	$0.8 \cdot 10^6$	0.90	0.133
	$0.8 \cdot 10^6$	0.92	0.120
Flow field survey (Prowim)	$0.8 \cdot 10^6$	0.85	0.168

Results and discussions

Balance measurements on PROWIM

During these tests several parameters were changed like : wing angle of attack, propeller thrust and flap deflection. In all cases with deflected flaps combinations of ($\delta_{fi} > 0, \delta_{fo} < 0$) and ($\delta_{fi} < 0, \delta_{fo} > 0$) were made. The purpose of this procedure was to adapt the lift distribution such that lower overall induced drag would be produced through lift enhancement at the UBS and a decrease at the DBS. Since a change in flap setting in general shifts the zero lift angle of attack, comparing points of equal lift-values would produce data points at different α To prevent a modification of the propeller thrust and slipstream characteristics the flaps angles were selected such that the lift coefficient remained constant for the same wing angle of attack. Since the forces on the propeller could not be measured separately the effective thrust was determined through a bookkeeping procedure. In this case the thrust of the propeller is defined as the difference in tangential force between the prop on (wnp) and prop off (wn) configuration. To determine the wing effect on the thrust, the propeller rotational speed was measured at windmill conditions for variable wing angle of attack with and without a constant propeller angle of attack with reference to the undisturbed flow direction. For all situations the windmill advance ratio remained constant. The constancy of the power delivered by the model motor during these tests underlines the fact that no change in thrust occurred. This check was only made for the propeller positioned at $x_p/c = -0.71$ For other streamwise positions an alternative procedure was followed as will be explained further on.

The database obtained from the balance measurement is very extensive therefore in this section only the results of a very small part is presented.

The thrust coefficient for the PROWIM test are quite low, nevertheless the effect of the propeller is clearly visible in fig. 2. The lift coefficient of the model increases with wing angle of attack due to both the generation of propeller normal force and the increased dynamic pressure in the slipstream. The propeller not only alters the wing lift, it influences the drag as well. With an elliptic-

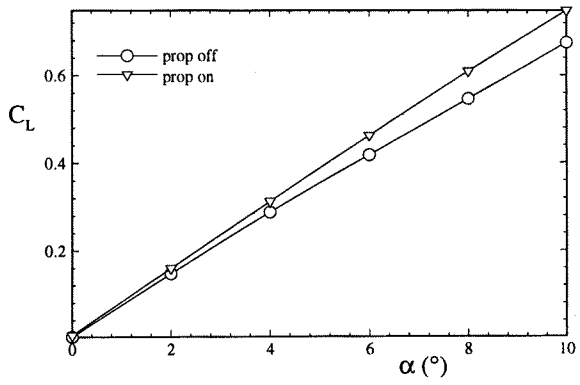

Figure 2: Lift coefficient of PROWIM versus α with and without running propeller, $J = 0.85$

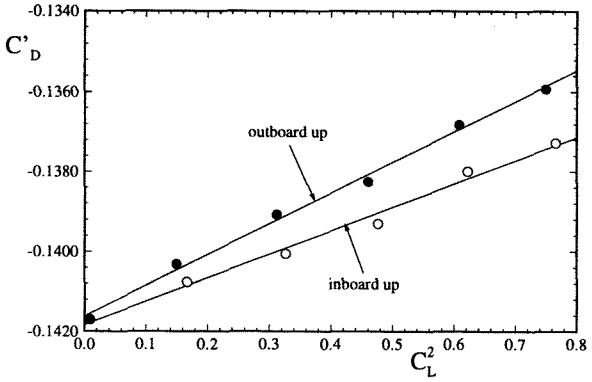

Figure 3: Effect of propeller rotation direction on the drag coeficient C'_D of PROWIM, $J = 0.85$, $y_p/b/2 = 0.468$

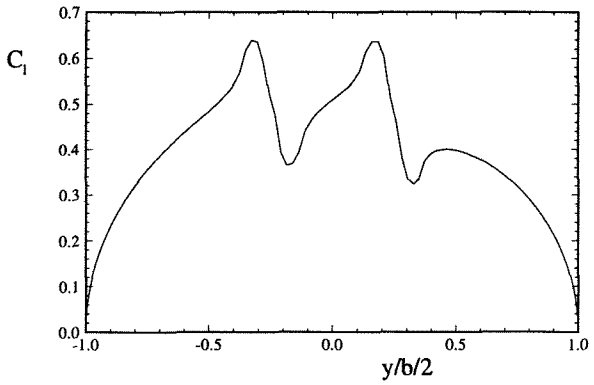

Figure 4: Typical optimized lift distribution for a Fokker 50-like propeller wing configuration (high speed case)

like lift distribution the inboard up rotating propeller should produce lower (induced) drag than the outboard up rotating propeller. As can be seen from fig. 3 indeed a remarkable gain in performance (through effective drag reduction) can be found when comparing propeller inboard up rotation and outboard up rotation. Here the effective drag coefficient C'_D is defined as :

$$C'_D = C_{D_{propon}} - C_{D_{propoff}} \quad (1)$$

This effect is enhanced with the propeller positioned at a spanwise position where the lift distribution is steeper (e.g. the wing tip area) as will be shown later. The effect of the propeller rotation direction is important since almost all twin-engine propeller powered aircraft have co-rotating propellers which introduce secondary drag forces due to trimming of the aircraft with asymmetrical aerodynamic loading (rolling and yawing moment, side force). Hence, it is evident that introduction of two inboard up rotating propellers should improve the performance significantly from aerodynamical point of view.

As described earlier by Veldhuis [6] the optimum lift distribution of the wing with active tractor propeller is far from elliptical. A typical lift distribution optimised for minimum induced drag is given in fig. 4 For a IUR propeller apparently a high lift coefficient is needed inboard and a much lower value at the outside. To check this optimization technique experimentally some PROWIM-tests were performed with flaps deflected differentially thus approximating the required lift distribution. In fig. 5 the effective drag versus the wing angle of attack is given for two combinations of flap settings. Clearly a reduction of the effective drag can be realized when introducing an adaptation of the lift distribution. Of course usage of flap deflection is not the appropriate method to optimize the wing lift distribution. Since leading edge and trailing edge of the wing are normally kept straight and the airfoil type (and camber) will not change strongly in spanwise direction,

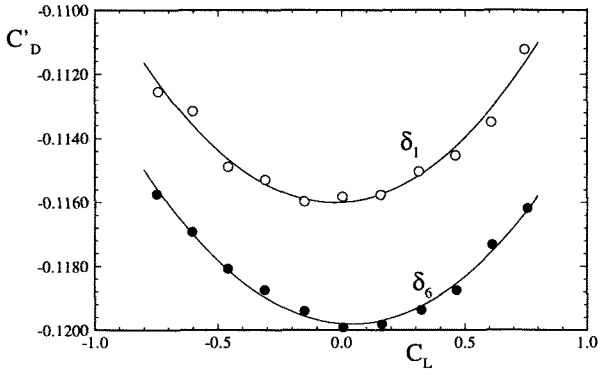

Figure 5: Influence of differential flap deflection on the effective drag polar of PROWIM, $J = 0.85$ ($\delta_1 : \delta_{fi} = 0°, \delta_{fo} = 0° \mid \delta_{fi} = 4°, \delta_{fo} = -4.52°$

the most attractive way to generate the optimum wing lift distribution may be an adaptation of the wing twist distribution. Due to deformation of the airfoil shape, as a result of wing twist, a combination of twist and variation of section shape will in practice be employed.

Pressure measurements on PROWIM

To get some indication about the extent of the slipstream influence on the wing, surface pressure measurements were carried out. In fig. 6 and 7 typical chordwise pressure distributions show the effect of the propeller at its "normal" position ($x_p = -0.71, y_p/b/2 = 0.469, z_p/c = 0.0$). The laminar separation bubble at approximately 5% c which is present for the measurements with the propeller off is completely removed when the slipstream is present. The turbulent flow introduced by the propeller apparently has a strong influence on the development of the wing boundary layer (Miley [19]). The increase in local lift

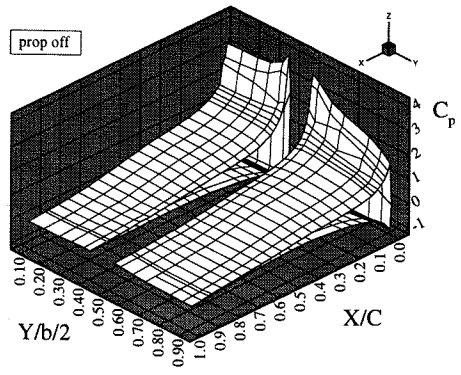

(a)

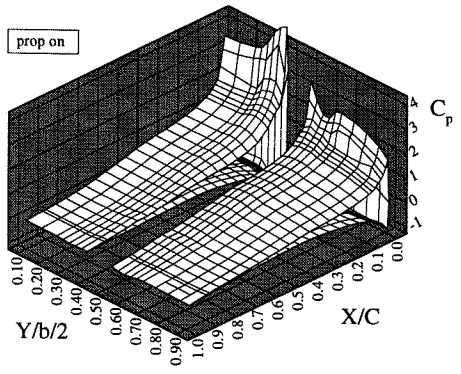

(b)

Figure 6: Typical surface pressure distribution of PROWIM at $\alpha = 10°$, (a) prop off, (b) prop on

for the UBS, due to increased dynamic pressure and increased local angle of attack is clearly visible. Note that the stagnation pressure is higher than its normal value of 1.0 found for the configuration without the running propeller. As shown in the 3-dimensional representation of the pressure distribution for the prop off case the nacelle influences the local onflow of the wing. Due to the increased velocity on both sides off the nacelle peaks in the local pressure distribution are found. The chordwise pressures were integrated to give the local values of normal and tangential coefficient. The latter excludes of course the contribution of friction forces on the wing surface which generally increase on the part washed by the slipstream.

Due to both the effects of total pressure rise within the slipstream and the propeller induced swirl velocity the distribution of normal force coefficient and tangential force coefficient is strongly distorted.

Fig. 8 and 9 show that a negative overall drag contribution is possible for the inboard up rotating propeller due to increased leading edge suction visible especially at the UBS of the nacelle. Thus the key to reduction of the drag would be to enhance the effects

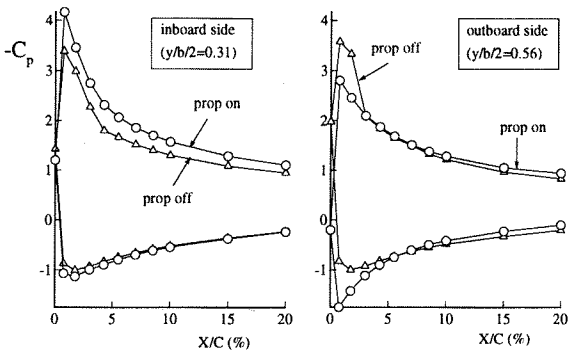

Figure 7: Leading edge pressure distribution of PROWIM at $\alpha = 10°$

on the UBS and deminish them at the DBS. When comparing the normal force coefficients in fig. 8(a) and 9(a) a clear difference is found going from wing root to wing tip. For $\alpha = 10°$ the decrease of the wing normal force is at the DBS is much smaller if not absent due to the opposite effects of the axial velocity and rotational velocity contributions. Consequently the wing's efficiency factor e, which is directly related to the lift distribution and which is normally independant of angle of attack now changes with this angle.

Effects of propeller position

Spanwise position The spanwise gradient in the lift distribution, at the position where the slipstream washes the wing, plays an important role with respect to the possible performance benefits introduced by the propeller. This was already shown by Kroo [1] and Miranda & Brennan [2] who placed the propeller at the extreme position namely the wing tip. Takallu et al. [7] who investigated the effects of the propeller located at a more realistic spanwise position state that changes in nacelle position and inclination have very little effect on the performance for the cruise wing configuration. In the next sections it will be shown that this statement needs to be reviewed.

First of all the influence of spanwise propeller position was investigated. For these tests the nacelle was disconnected from the wing and mounted on a strut which could be traversed in any direction with respect to the wing (APROPOS). Effects of streamwise, spanwise and vertical positions of the propeller with respect to the wing leading edge were tested and the aerodynamic characteristics of the configurations were analysed. In fig. 10 and 11 the results of some balance measurements with the propeller installed at several spanwise positions is given for $T_c = 0.120$. The different curves corresponds to various vertical positions of the propeller which will be discussed further on in more detail. As

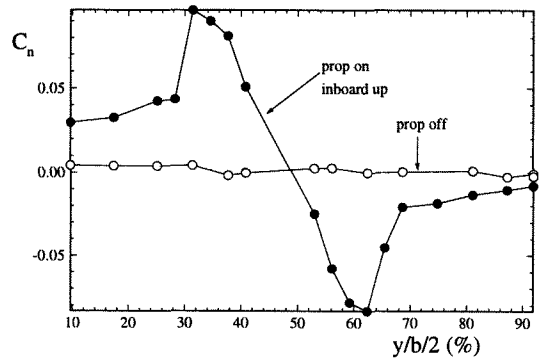

(a) $\alpha = 0°, C_n$

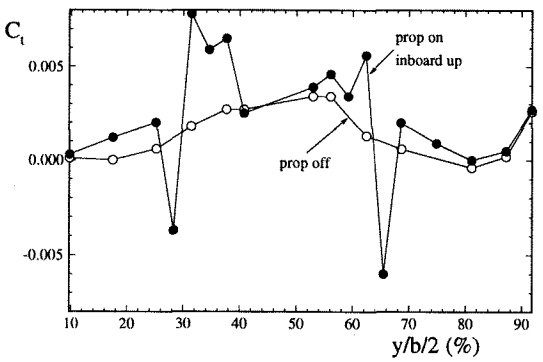

(b) $\alpha = 0°, C_t$

Figure 8: Effect of the propeller on the normal force and the tangential force coefficient of PROWIM, $\alpha = 0°$, $J = 0.85$

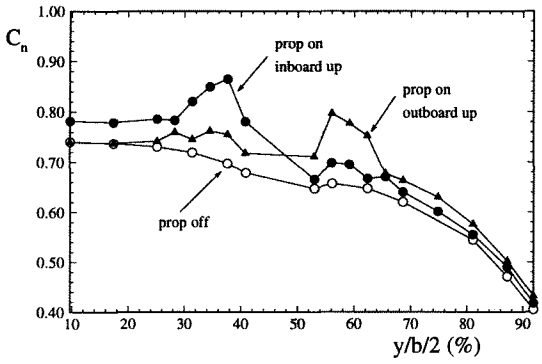

(a) $\alpha = 10°, C_n$

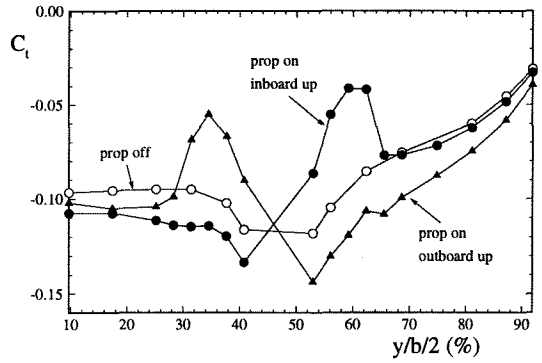

(b) $\alpha = 10°, C_t$

Figure 9: Effect of the propeller on the normal force and the tangential force coefficient of PROWIM, $\alpha = 0°$, $J = 0.85$

expected the performance of the wing improves when moving the propeller in the direction of the wing tip. Apparently the vorticity field (swirl) induced by the inboard up rotating propeller attenuates the wing tip vortex influence. As a result the lift increases while the drag decreases going to the tip (fig. 11). Tests with the propeller rotating in the same direction as the wing tip vortex (outboard up) reveals negative effects, as expected. Tests at several angles of attack have shown that the effect at the wing tip is maximum when the slipstream centerline is exactly in line with the wing tip vortex.

Vertical position As described in the previous section, moving the propeller in the vertical direction has a remarkable influence on the performance of the wing. For realistic spanwise locations a high position is beneficial with reference to the wing lift/drag ratio, mainly due to lift enhancement introduced by the dynamic pressure increase at the wing upper surface. To study this phenomenon in more detail additional balance measurements were performed for variable z-positions of the propeller. During these tests the propeller was located at $y_p/b/2 = 0.281$ and $x_p/R = -1.44$. Both low thrust ($T_c = 0.133$) and high thrust conditions ($T_c = 0.77$) were analysed. In fig. 12 the behaviour of the lift and the drag coefficient are presented versus the vertical propeller position. For $\alpha = 4°$ the maximum value of the lift is reached for $z_p/R = 0.51$. This configuration is visualized in fig. 13. Here, the average dynamic pressure increase at the wing position reaches its maximum value. For lower values of z_p/R the pressure deficit in the core of the slipstream, which is caused by the nacelle wake results in lower lift coefficients. The fact that the lift does not increase for $z_p/R = -0.51$ indicates that the swirl velocity in the slipstream also plays a part in the lift enhancement process. In case the slipstream centreline is located underneath the wing chord reference line the inboard up rotating propeller strengthens the crossflow at the lower wing surface in the direction of the wing tip. Thus the overall wing lift is reduced. Note that another difference between the high and low position of the propeller is caused by the inflow into the slipstream. For high z_p/R-values this

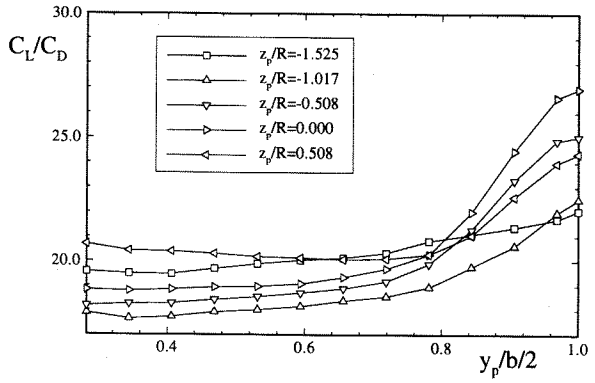

Figure 10: Influence of spanwise propeller position on the lift/drag ratio of PROWIM, $\alpha = 4.2°$, $\alpha_p = 0°$, $J = 0.92$

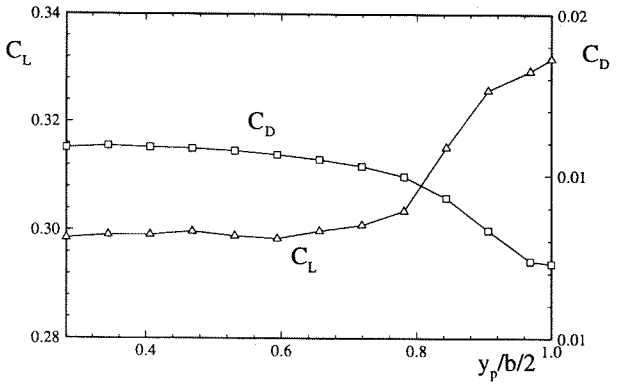

Figure 11: PROWIM lift and drag coefficient versus propeller spanwise position $\alpha = 4°, \alpha_p = 0°, J = 0.92, z_p/R = 0.0$

results in a local wing angle of attack increase and a lift increment; for the lower z_p/R-values an opposite effect occurs (fig. 14). Sumarizing one can state that the wing may benefit from the presence of the propeller since C_L/C_D rises for the higher propeller position. In fig. 15 the performance of the wing, indicated by its C_L/C_D value, is given as a function of the propeller vertical position. These trends seem to confirm observations by other researchers that the projection of the propeller plane on the wing strongly influences the local wing lift.

Streamwise position Several windtunnel investigations indicate the necessity to take into account the strong aerodynamic interactions that can occur for unconventional positions of the propeller. One important configuration is when the propeller is located close to lifting surfaces. Especially for over-the-wing propeller configurations favourable interference effects could be obtained. Johnson & White [17], for example,

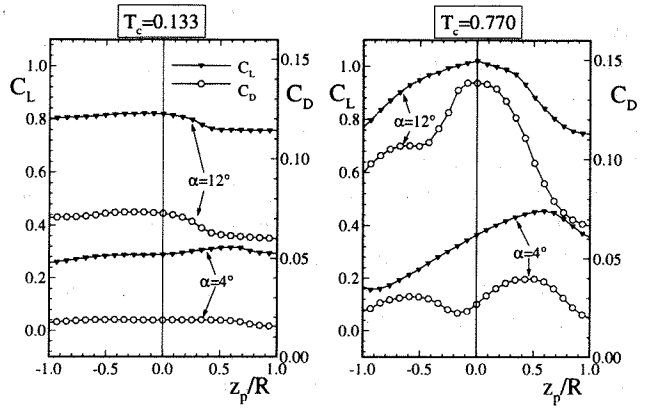

Figure 12: Lift and drag coefficient versus propeller vertical position (APROPOS)

found significant performance improvements at a climb lift coefficient of 0.7 over designs which had the propeller mounted in front of the wing. The aerodynamic effects of an over-wing propeller were also studied by Cooper et al. [18]. They also showed that beneficial interaction effects were attainable for wings with deflected flaps. Remarkable and unexpected is their conclusion that the efficiency of the propeller was maintained. Williams et al [10], used a full 3D aircraft model to check the effects of an over-the-wing propeller under climb an cruise conditions. With this arrangement a clear reduction of the wing drag was obtained for increasing thrust coefficient. A beneficial side effect of their configuration was that the aft location the propulsion system produced stabilizing pitching moment contributions originating from the propeller normal forces located behind the aircraft c.g.

Since these conclusions hold interesting options for optimisation of tractor propeller/wing combinations further research for this particular location of the propeller is recommended. Bearing this in mind, the effect of the streamwise position was also investigated using the APROPOS test setup. During these experiments is was noticed that no significant influence of the propeller streamwise placement was found for positions well

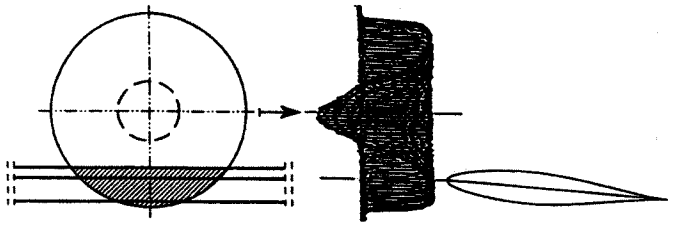

Figure 13: Propeller/wing configuration for maximum lift increment due to the propeller slipstream, $\alpha = 4°$

in front of the wing leading edge. For the propeller placed very close to the wing, i.e. in an over-the-wing fashion, however, remarkable strong effects were found. Although the wing angle of attack may have an important influence of the magnitude of the over-the-wing propeller effect, this investigation was only performed at $\alpha = 4.2°$. Significant gains in lift and reductions in drag were found when positioning the propeller above the wing. In fig. 16 wing lift and drag coefficient are presented versus the dimensionless streamwise position of the propeller. The propeller plane was perpendicular to the undisturned flow i.e. and it was positioned to give a tip clearance of 17.5% of wing chord above the wing $\frac{1}{4}c$ line. Where the influence of the streamwise position is noticeable but small for the low thrust coefficient, the high thrust condition results in very high lift and even negative wing drag for propeller positions well above the wing. The favourable effects of the propeller become maximum, with regard to the wing drag, for propeller locations around $x_p/c = 0.40$ and they decrease when moving the propeller further backward. The lift though still increases in this direction, a result which is subscribed by Williams et al. [10] and Takallu et al. [7]. The key aerodynamic feature is the propeller induced flow over the wing causing increased lift and reduced drag. Especially the strong inflow into the propeller disk which enhances the leading edge suction has a strong influence on this drag reduction.

In general, for propeller positions close to the wing, reductions in wing drag might be associated with a drop in propeller efficiency. For this reason a performance indication obtained from the combined configuration in which both the propeller and the wing are combined is more representative for the overall benefits. Therefore the drag change of the wing is treated as a propeller thrust augmentation. In this case an effective propulsive efficiency can be chosen :

$$\eta_{eff} = \frac{T_c - \Delta C_D \frac{S}{D^2}}{P_c} \qquad (2)$$

Since no internal balance was present to measure the thrust of the propeller separately, the total pressure jump across the disk was measured. Integration across the disc then yields the effective thrust of the propeller. This was done for two positions of the propeller denoted A and B at $x_p/c = 0.50$ and $x_p/c = -0.71$ respectively. For the high thrust condition ($J = 0.43$) values of $T_c = 0.7701$ and $T_c = 0.7746$ were found for positions A and B respectively. As expected the thrust coefficient for A is somewhat lower due to the increased flow velocity over the wing upper side. Fortunately the power required for this T_c-value is also reduced (fig. 17). Apparently, the effect of the wing proximity on the propeller performance is relatively small. If we look at the the value of η_{eff} we find that it changes from 0.346 at position B to 0.408 at position A. For the low thrust case this value changes from $\eta_{eff} = 0.793$ at position B to $\eta_{eff} = 0.851$ at position A. This is a remarkable performance improvement. Again is should be noted that the over-the-wing positioning of the propeller reveals an increment of the lift coefficient and a reduction in drag. Takallu et al. [7] however always found a drag rise.

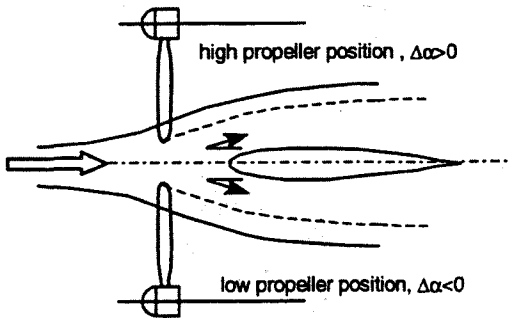

Figure 14: Effect of propeller vertical position on the local wing angle of attack due to the inflow into the slipstream.

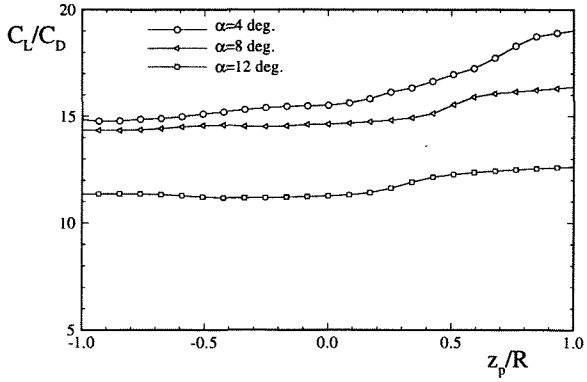

(a) $T_c = 0.133$

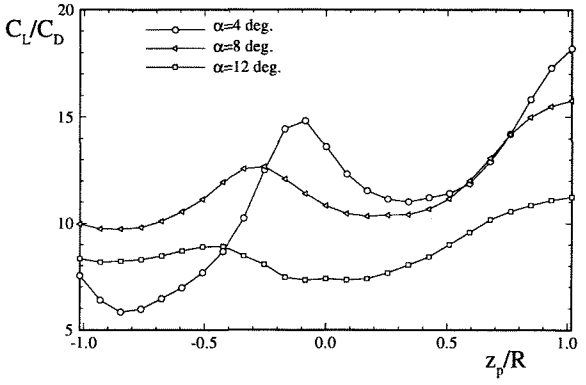

(b) $T_c = 0.77$

Figure 15: Wing C_L/C_D versus propeller vertical position

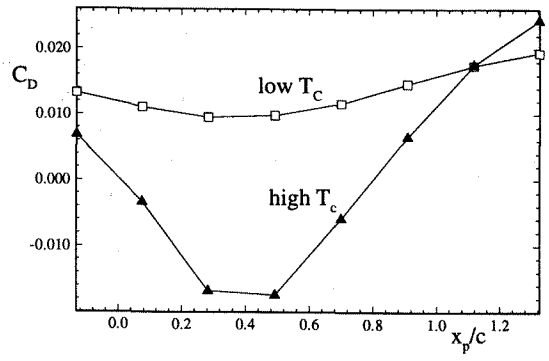

(a)

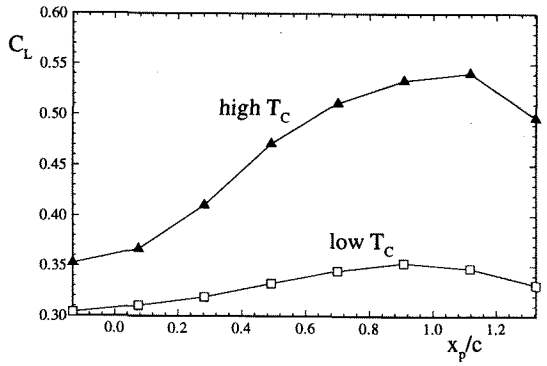

(b)

Figure 16: APROPOS drag (a) and lift (b) coefficient versus streamwise propeller position (low T_c : T_c = 0.133, high T_c : $T_c = 0.77$

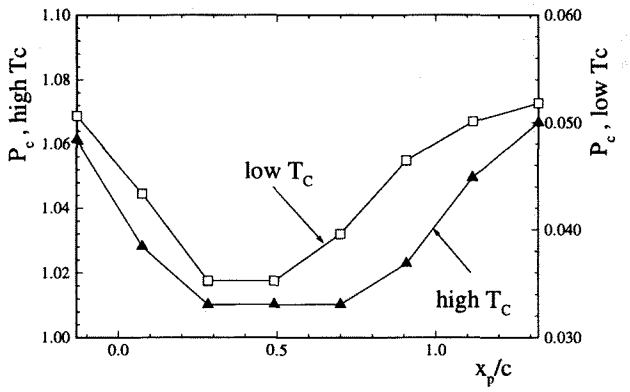

Figure 17: Model motor power coefficient versus streamwise propeller position, $\alpha = 4.2°$.

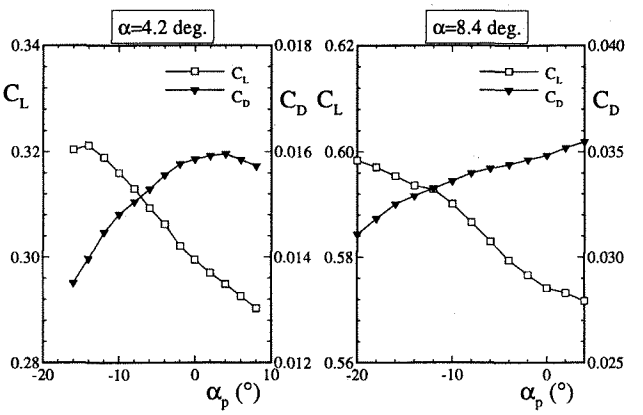

Figure 18: Effect of the propeller angle of attack on the wing lift and drag of APROPOS

Although some propeller positions seem to result in considerable performance benefits it should be noted that connection between the nacelle and the wing generally reduces the lift, changes the lift curve slope and increases the drag. Therefore practical implementation of an over-the-wing propeller arrangement certainly requires further detailed research.

Effect of propeller inclination

As described previously, a fixed position of the propeller with reference to the wing brings about a strong deformation of the slipstream symmetry when the wing is given a positive angle of attack. In principle this causes detrimental effects with regard to the induced drag of the wing. When looking at the propeller itself it is important to understand that the wing generally introduces upflow in the propeller disk area. Thus, the correct setting of the tilt down angle for minimum alternating loads on the blades depends typically on the streamwise position of the propeller. It should be noted that significant flow non-uniformity might also be introduced by the presence of the nacelle when it is positioned at some positive angle of attack. The fact that this has a negative effect on the propeller is another reason to explore further the advantageous effects of the PTD-configuration. Propeller thrust line tilt down may also be used to improve power-on longitudinal stability through reduction of in-plane normal forces. Normally the angle of incidence given to a propeller is limited to say 2°. In the next section however the possible performance benefits of much bigger angles will be analysed. Although all the tests with variable y_p- and z_p-positions were performed for several propeller incidence angles α_p only the results for $y_p/b/2 = 0.469$ and $z_p/R = 0.0$ are presented. In fig. 18 the lift and the drag coefficient are given versus α_p. Clearly tilting down the propeller improves the performance of the wing through an increase in lift and a reduction in drag. This results in a significant rise of the C_L/C_D ratio (fig. 19). Note that here the underlying cause is on principal different from the effect of vertical displacement of the propeller since now the velocity distribution in the

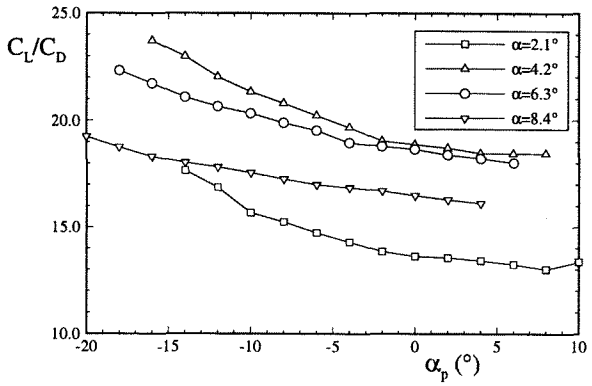

Figure 19: Wing C_L/C_D versus propeller angle of attack for several wing α, J=0.92

slipstream has undergone a major change (Veldhuis [6]). The experimental data are qualitatively in agreement with the results of an optimisation code used for preliminary design purposes described by Veldhuis [6]. This code also predicts remarkable performance benefits for PTD-configurations. Note that the (small) negative normal force acting in the propeller plane and the (small) reduction in effective thrust hardly reduces the positive effects. In contrast to the over-the-wing layout, an innovative configuration with application of propeller tilt down angles up to say 15° should not raise major problems from the structural point of view. Consequently, further analysis of the pros and cons of PTD-configurations is recommended.

Flow field survey

The flow generated by a propeller/wing configuration is very complex , therefore a succesfull optimisation with theoretical prediction techniques will only be sucessful if quite detailed field data are available. Of course the flow field data not only give information on the wing loading but are also of importance for the design of the empenage. One of the attempts to explain the different phenomena that occur when a propeller slipstream interacts with a trailing wing was made by Aljabri & Hughes [8]. Their analysis is however restricted to a 2 dimensional wing. Besides this, the flow field characteristics are mainly presented in the form of cross-flow vector plots, as used by many authors. Unfortunately this type of data not always contains enough information or may even produce a wrong perception of the real flow structure (Krämer et al [13]) The reason is that superposition of discrete vortices aligned in a certain manner can sometimes hardly be distinguished from the velocity field induced by a single vortex.

To better understand the balance and surface pressure data discussed earlier, a program of flow field surveys behind PROWIM was performed. In this section a small part of the first windtunnel experiments is presented. A detailed description of this flow field survey is given by Rentema [12].

Time-averaged slipstream and wake measurements were performed at 1 chord length behind the wing trailing edge. The propeller was rotating inboard up with an advance ratio of $J = 0.85$. To be able to analyse slipstream influence on the wing profile drag, induced drag and lift distribution a grid spacing of $2mm$ was chosen in both directions. This very fine grid was needed to apply the theory of Betz [14] and Maskell [15] to generate accurate integration of flow data over the wake area and to uncover enough detail of the flow field to draw qualitative conclusions.

Flow structure for the propeller off case

In fig. 20 the distribution of the total pressure coefficient is given for the the propeller on case at $\alpha = 0°, 4°$ and $10°$. The strong deficit which occurs in the wing wake and the wing tip vortex are clearly visible. Besides the total head loss behind the nacelle with the pressure tubes installed, there is a distinct effect of the horseshoe vortex at the wing/wall junction. For $\alpha = 4°$ and $10°$, when the wing generates lift, the total head loss in the tip vortex core becomes very pronounced. The wake starts to deform significantly for the higher angles of attack. Near the root, the wake of the wing shows a disturbance (see arrow in fig. 20(b)) which becomes larger at higher angles of attack. This is caused by a small streamwise gap between the trailing edges of the inboard flap and the wing. The fact that this small geometrical disturbance generates a measurable effect demonstrates the power of the flow field analysis. In fig. 21 and fig. 22 cross flow vectors are depicted for 2 flow cases. Although this type of graph is easily generated, even on-line during the measurements, it exhibits no significant additional information on the flow field compared to the axial vorticity plots shown further on. In fact the interpretation of the cross flow vectors may result in a completely wrong perception of the real flow field since distinct vortices can not be distinguished as shown in the example given by Krämer et al. [13]. In this respect the axial vorticity ξ, as presented in fig. 23 and 25, reveals more detail. For $\alpha = 0°$ two vortex pairs are visible originating from the horseshoe vortices generated by the nacelle/wing connection. At $\alpha = 4°$ the vortices with negative ξ merge and the field rotates in anti-clockwise direction due to the cross flow induced by the wing. Since the wing now produces lift the wake rolls up resulting in a strong vortex with very high ξ-value at the tip. Moving from the tip to the root the trailing vorticity becomes weaker. This is easily explained by considering the spanwise gradient of the lift which decreases when moving rootward.

Flow structure for the prop on case

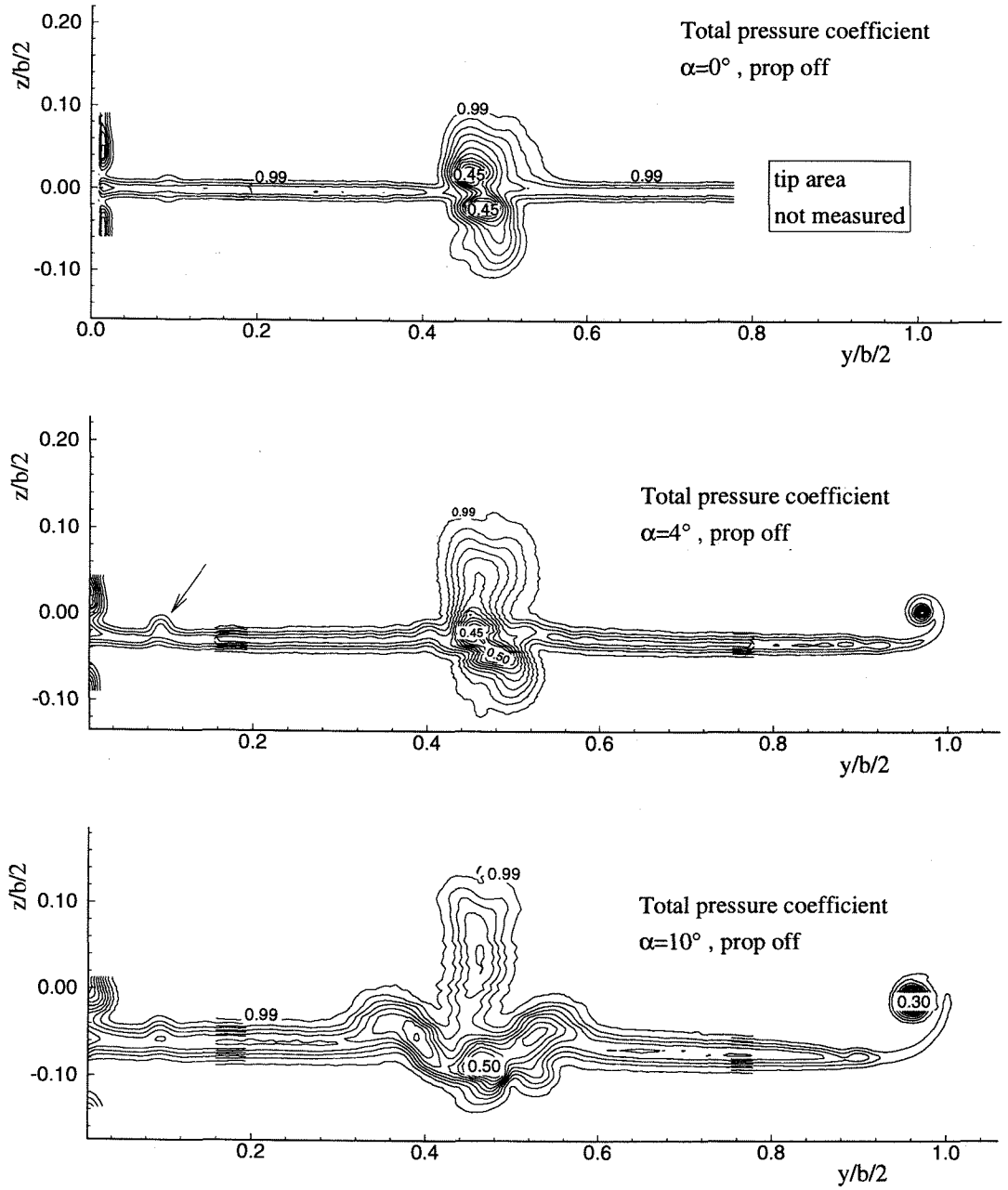

Figure 20: Total pressure coefficients for the propeller off case. The total pressure loss at the center of the figures is the result of the wake of the nacelle with installed total pressure probes at upper and lower side.

With the propeller running the structure of the flow field changes radically. As can be seen in the C_{P_t}-plots of fig. 24 a strong total head rise occurs in the slipstream. There are remarkable strong spatial gradients in total pressure towards the slipstream boundary. Apparently the diffusion of the vorticity between the propeller position and the survey plane is limited. This can also be seen in the axial vorticity plots of fig. 25 where distinct boundaries are visible. The wake of the nacelle is completely embedded in the slipstream which is substantially distorted by the wing. In fig. 26 a 3-dimensional view of the total pressure rise at $\alpha = 10°$ is given. Although this picture produces a nice qualitative view of the different phenomena that occur in the flow the contour plot of fig. 24 reveals more quantitative data. Here we see that the total pressure rise is higher at the side of the downgoing propeller blade due to the increased local blade angle of attack. The swirl generated by the propeller results in a slow rotation of the slipstream as indicated by the displaced

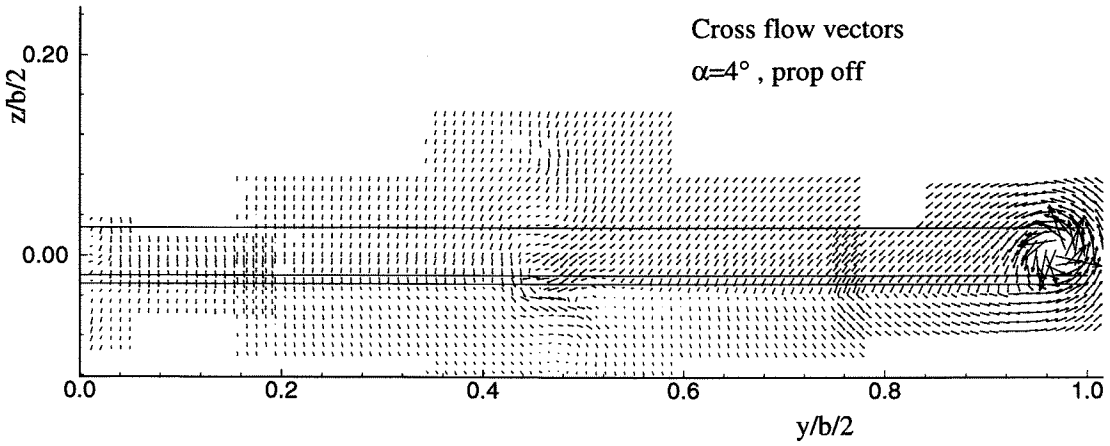

(a)

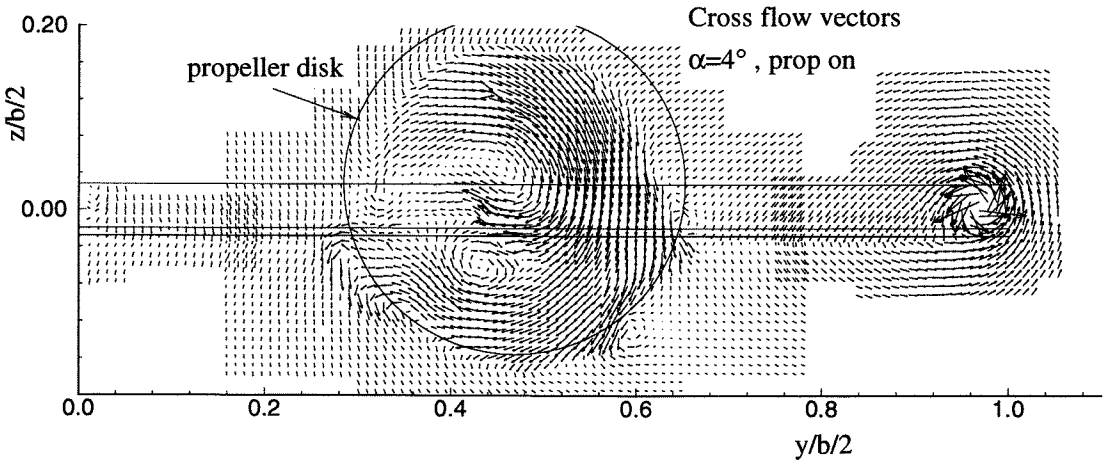

(b)

Figure 21: Cross flow vectors for $\alpha = 4°$, (a) prop off, (b) prop on.

total pressure field in fig. 24(c) where at $\alpha = 10°$ the peak total pressure value has moved in the propeller rotational direction. This, of course has implications for the aerodynamic load on trailing surfaces.

Although it is difficult to relate a ξ-peak in the survey plane to a corresponding spanwise coordinate on the wing, due to (unknown) wake deformation between the wing and the survey plane, the effects of the propeller blade tip vortices and the wing tip vortex are very pronounced.

When viewed from behind, the tips of the propeller blades produce anti-clockwise vortices. These vortices create a narrow zone with high positive x-values at the outer border of the slipstream. The root parts of the propeller blades produce negative vorticity which is spread out inside the nacelle wake area. As can be seen in fig. 24(a) for $\alpha = 0°$ the rotational symmetry of the slipstream is clearly influenced by the presence of the wing. The boundary seems to be sheared at the passage of the wing so that the slipstream boundaries at the upper and lower wing surface are at different spanwise stations. A convenient explanation of this phenomenon can be found in the way the slipstream influences the wing lift distribution. Fig. 25 shows that strong vorticity is shed from the junction of the wing surface and the edge of the slipstream, which is indicative of the high gradient of spanwise load on the wing. To explain the effect the vorticity is considered as being contained in 3 discrete vortices (fig. 27). As a result both slipstream halves shift in opposite spanwise directions near the intersections between the wing and the slipstream outer boundary. The areas with negative ξ-values at these locations confirm this explanation. Also the clockwise rotating center vortex with positive ξ is clearly visible in fig. 25. At $\alpha = 10°$ both slipstream halves have shifted in opposite directions due to the strong influence of the wing tip vortex. Although the 5-hole probe measurements were all performed at a

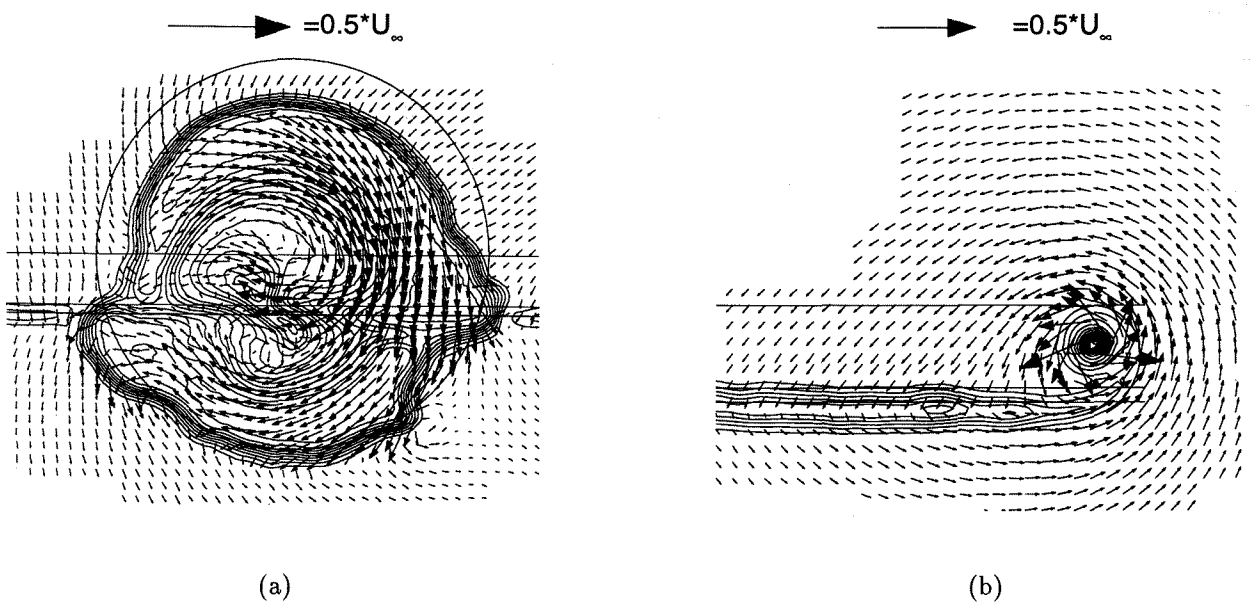

(a) (b)

Figure 22: Cross flow vectors combined with total pressure contours for $\alpha = 4°$, (a) slipstream region, (b) tip region.

rather low thrust coefficient the contraction of the slipstream is still visible, especially at $\alpha = 0°$ in fig. 24. Summarizing these results it should be stated that the deformation which occurs in the wake is strongly related to the lift distribution of the propeller/wing combination. Therefore further research is recommended to analyze the effects of different slipstream geometries on the calculation results of CFD-codes which incorporate propeller flow.

Quantitative wake analysis

Following the theory presented by Betz [14] and Maskell [15] a quantitative analysis of the flow field data was performed. The purpose of these investigations was to check the capabilities of the theoretical model in testcases with running propellers and to acquire more detailed information about the swirl recovery effect of the wing. In this section only a brief review is given of the theoretical model for the analysis of profile drag, induced drag and lift from the measured flow field data. A more comprehensive discussion is offered by Rentema [12].

Drag integrals Starting with the moment equation for an arbitrary object placed between windtunnel walls, Betz and Maskell derived the following relation for the total drag :

$$D = \iint_W (H_\infty - H_2) + \frac{1}{2}\rho(u_2^* - u_2)(u_2^* + u_2 - 2U_\infty)\,dy\,dz - 2\rho u_b^2 + \frac{1}{2}\rho \iint_S (v_2^2 + w_2^2) - (v_1^2 + w_1^2)\,dy\,dz \quad (3)$$

Here index 1 and 2 refer to survey planes $S1$ and $S2$ upstream and downstream of the model respectively. The first to terms are considered by Betz as the *profile* drag while the last term is supposed to be the *vortex* drag or *induced* drag. It should be noted that for the case where a propeller is running the energy supply to the flow increases the value of the total pressure H_2, which means that the profile drag may become negative. The first part of eq. (3) is limited to the wake through the introduction of the Betz'-velocity u^* which differs from u only in the wake area :

$$H_\infty = p + \frac{1}{2}(u^{*2} + v^2 + w^2) \quad (4)$$

The term u_b is the socalled blockage velocity for which Maskell derived the following relation :

$$u_b = \frac{1}{2S} \iint_W (u_2^* - u_2)\,dy\,dz \quad (5)$$

The problem of the second integral of eq. (3) is that it must be evaluated over the entire cross section of the windtunnel. Maskell [15] and Wu et al. [16] however solved this problem by introducing two scalar function defined by :

$$v = \frac{\partial \psi}{\partial z} + \frac{\partial \phi}{\partial y}$$
$$w = -\frac{\partial \psi}{\partial y} + \frac{\partial \phi}{\partial z} \quad (6)$$

Furthermore the continuity equation is used :

$$\frac{\partial v}{\partial y} + \frac{\partial w}{\partial x} = -\frac{\partial u}{\partial x} = f \quad (7)$$

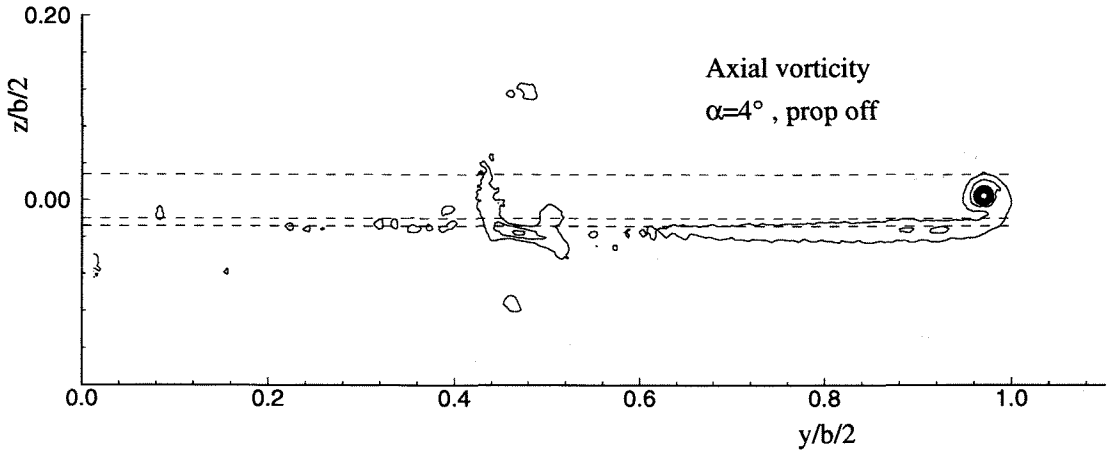

(a)

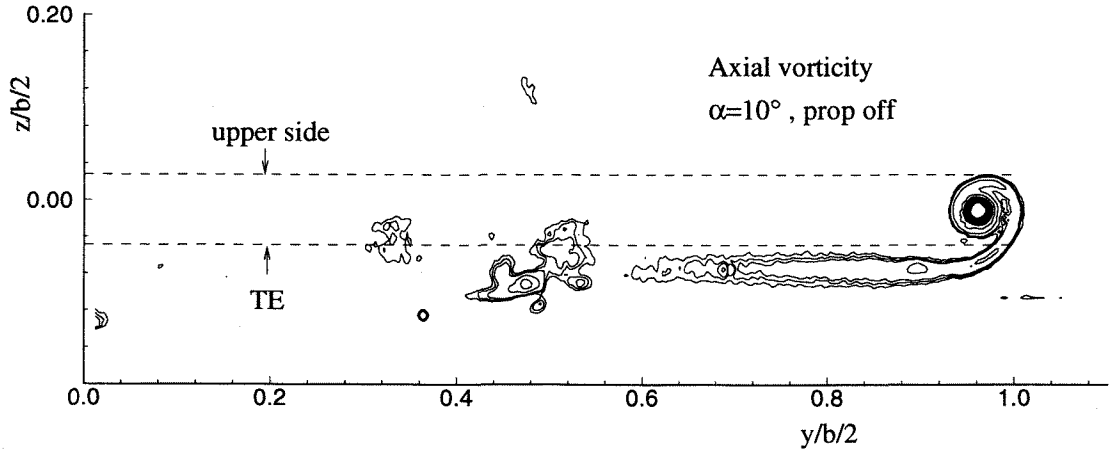

(b)

Figure 23: Axial vorticity ξ for the propeller off case.

and the vorticity vector :

$$\vec{\omega} = \vec{i}\xi + \vec{j}\eta + \vec{k}\omega \tag{8}$$

Combing equations (7) and (8) leads to the following expressions :

$$\begin{aligned} \frac{\partial^2\psi}{\partial y^2} + \frac{\partial^2\psi}{\partial z^2} &= -\xi \\ \frac{\partial^2\phi}{\partial y^2} + \frac{\partial^2\phi}{\partial z^2} &= f \end{aligned} \tag{9}$$

Without further proof it is stated that with a combination of equations (6) and (9) the second integral of eq.(3) and can be transformed into a simplified equation for the vortex drag coefficient :

$$D_v = \frac{1}{2}\rho \iint_W \psi_2\xi_2 \, dy\, dz - \frac{1}{2}\rho \iint_W \phi_2 f_2 \, dy\, dz \tag{10}$$

where index 2 refers to the survey plane at a certain distance behind the windtunnel model. In general the contribution of the second integral is negligible outside the wake (de Leeuw [11]).

The profile drag and the vortex drag can now be calculated using (3) and (10). The solution of the Poisson equations (9) is performed with a standard Solver applying the right boundary conditions (Rentema [12]).

Lift integrals The lift of the model can also be evaluated from the wake data following the classical wing theory. From the conservation of vertical momentum in the control volume bounded by the windtunnel walls and two transverse planes upstream and downstream of the lifting system it follows that the total lift

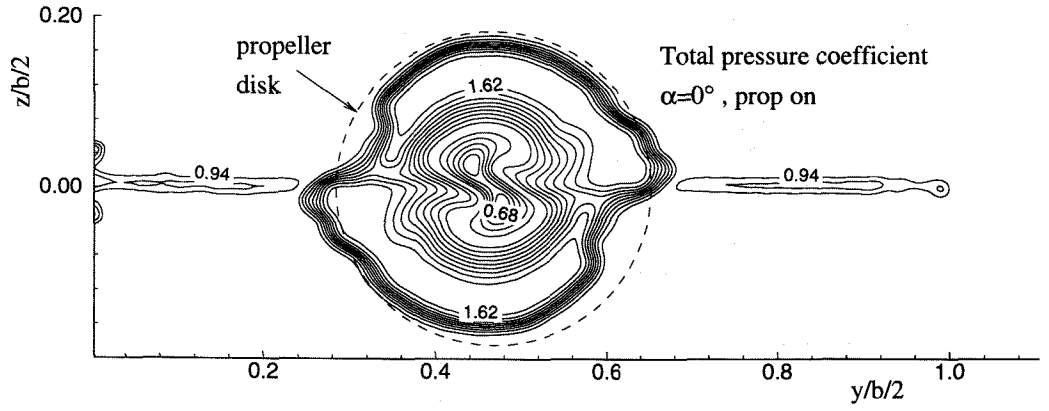

(a)

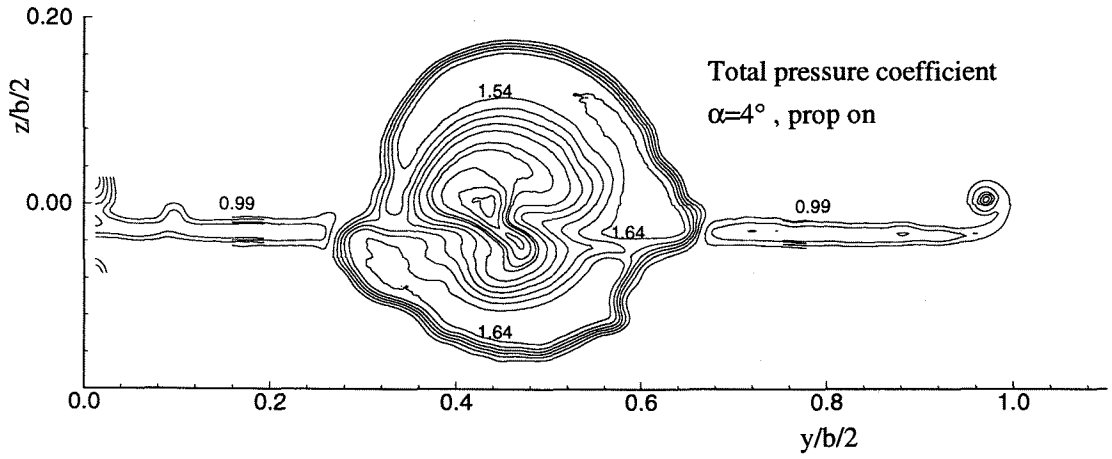

(b)

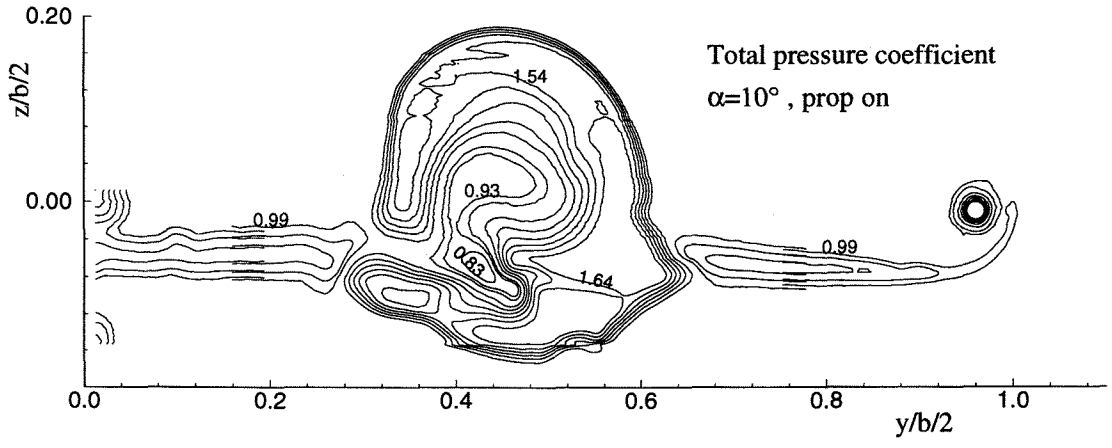

(c)

Figure 24: The total pressure coefficient C_{P_t} for the propeller on case.

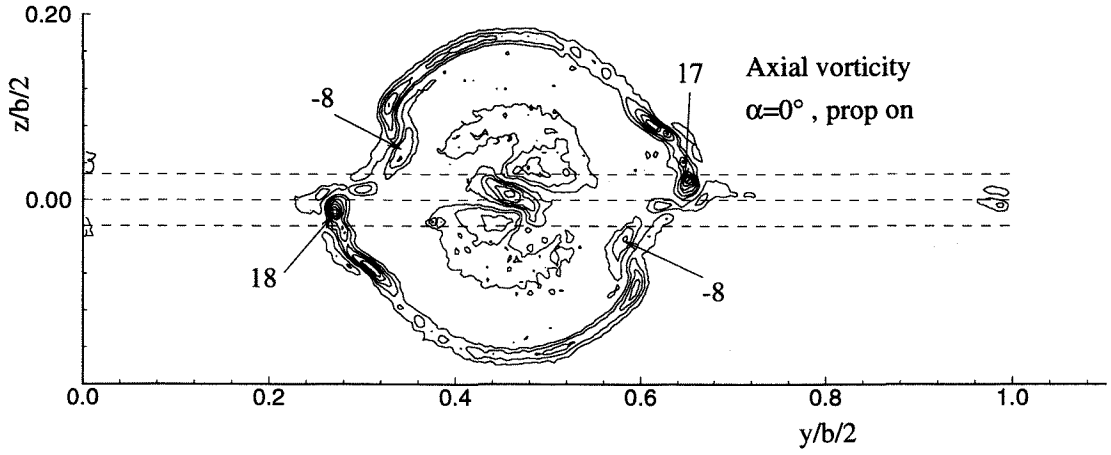

(a)

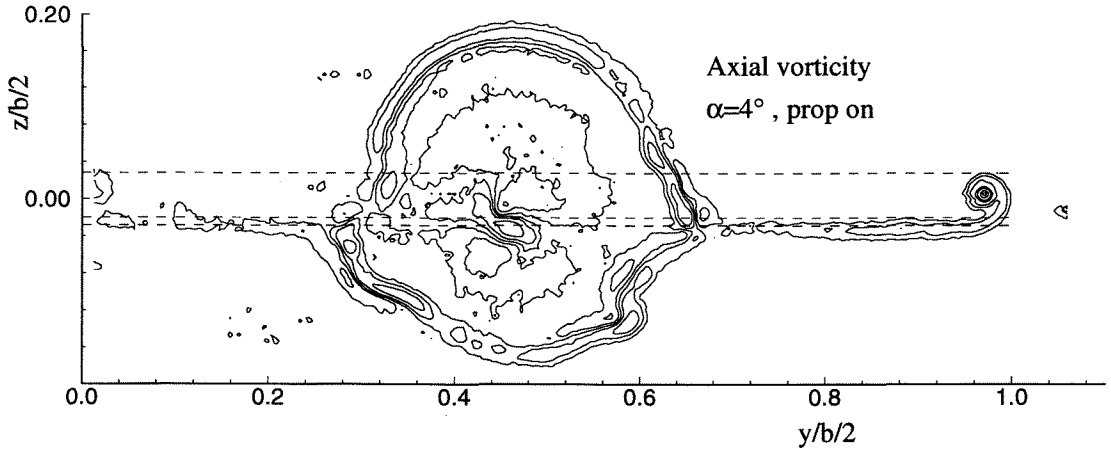

(b)

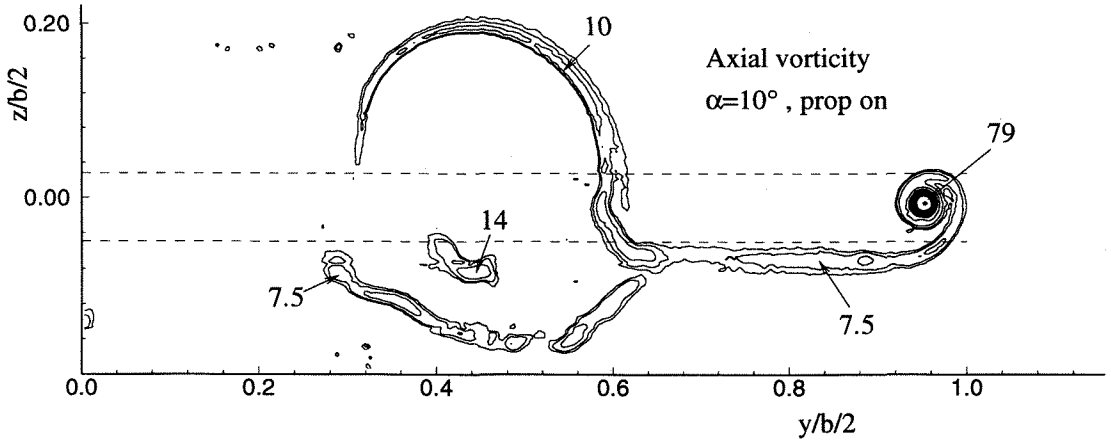

(c)

Figure 25: Axial vorticity ξ for the propeller on case.

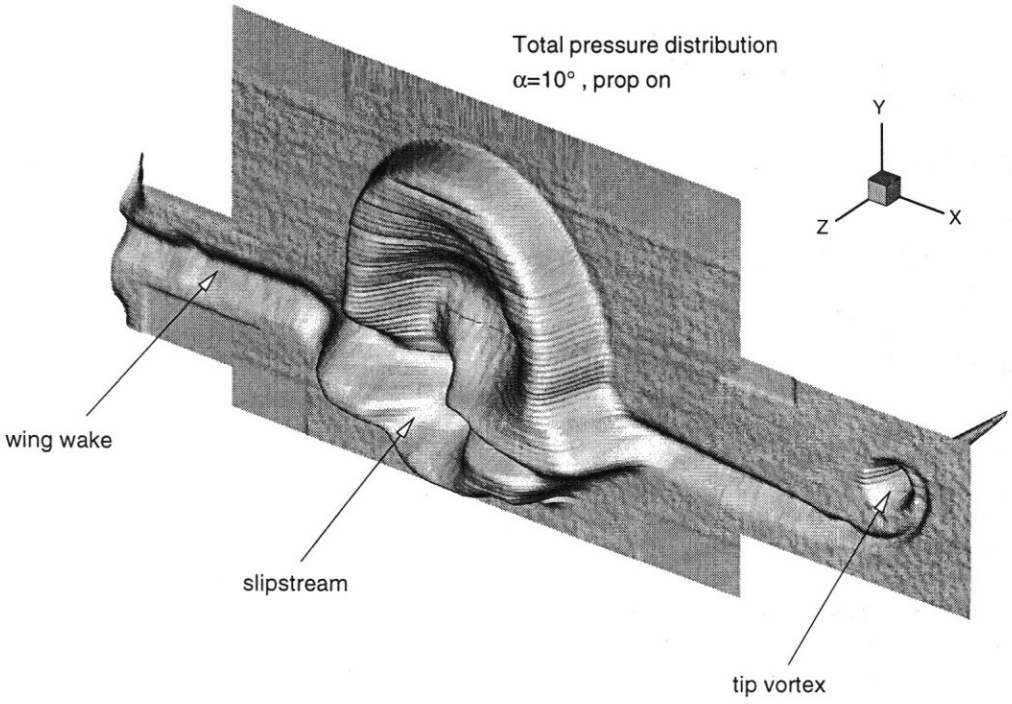

Figure 26: Three-dimensional view of the distribution of the total pressure coefficient at $\alpha = 10°$, showing the effect of the wing wake, the slipstream and the tip vortex.

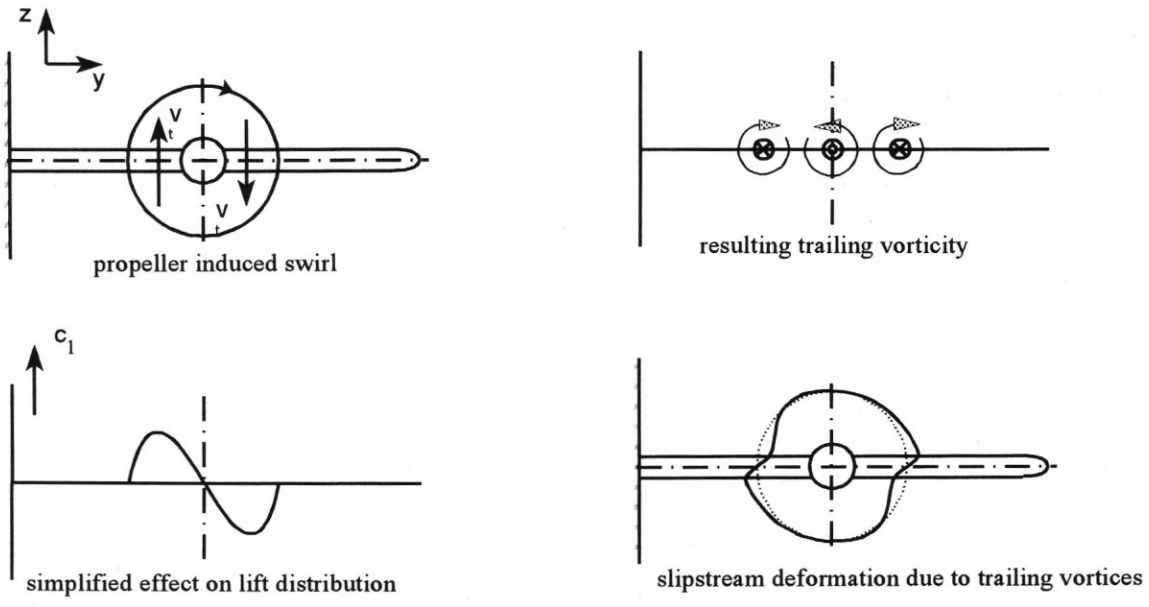

Figure 27: Simple explanation for the spanwise shearing of the propeller slipstream induced by trailing vorticity

can be written as :

$$L = \iint_{S_u} p\,dS - \iint_{S_l} p\,dS - \iint_{S} wU\,dS \qquad (11)$$

Following a procedure similar to the that employed for the derivation of the drag formula (3), Maskell [15] produced the following lift integral :

$$L = \rho U_e \iint_{W} \xi y\,dS + \rho \iint_{W} (u_2^* - u_2) w_2\,dS \qquad (12)$$

where the contribution of the second term turns out to be negligible in practice. The local lift coefficient can also be found from the measured axial vorticity ξ :

$$C_l = -\frac{2}{Uc} \int_{y_1=y}^{\infty} \int_{z=-\infty}^{\infty} \xi\,dz\,dy_1 \qquad (13)$$

It should be noted that the wake of the wing deforms which means that from the shed vorticity the direction and the location of the inducing (normal) force can not be determined exactly.

Comparison with surface pressure measurements Although the wing has some straightening effect on the flow the basic circular shape of the slipstream is maintained and substantial swirl velocities remain within the slipstream downstream of the wing. This becomes clear when the lift distribution found from integration in the wake is examined.

In fig. 28 and 29 the distribution of the local lift, represented by eq. (13), is presented for $\alpha = 4°$ and $\alpha = 10°$ together with the results of the integrated surface pressure measurements.

A small difference between the lift acquired with both techniques outside the slipstream area is notable in all figures. The reason for this discrepancy is still unclear but is expected to be a result of a cumulation of several small errors within both measurements. Further research will be performed to improve both experimental techniques.

The most striking difference however between the flow field survey curves and the results of the surface pressure measurements is the opposite effects in the area washed by the slipstream. The latter represents the pressure effects at the wing only, hence no contribution of the lift forces that act on the propeller blades are incorporated in the data. The flow field data however contain the lift contribution of the complete configuration. Obviously the normal forces acting in the propeller plane exceed the lift variations at the wing which are generated by the slipstream. This means in fact that a considerable swirl is still present in the slipstream after passage of the wing. Here again it is important to note that the wake position, where a certain value of the local lift is found, cannot be directly connected to a known wing spanwise location. On the other hand, a separate investigation of

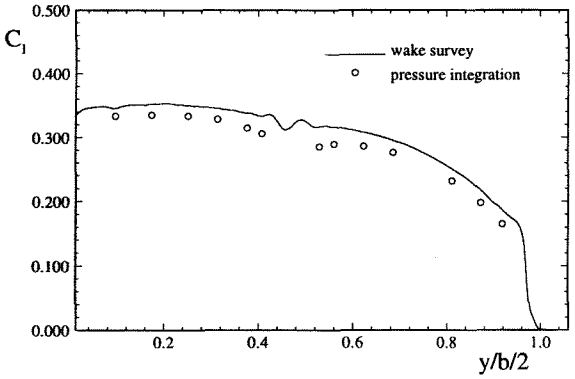

(a)

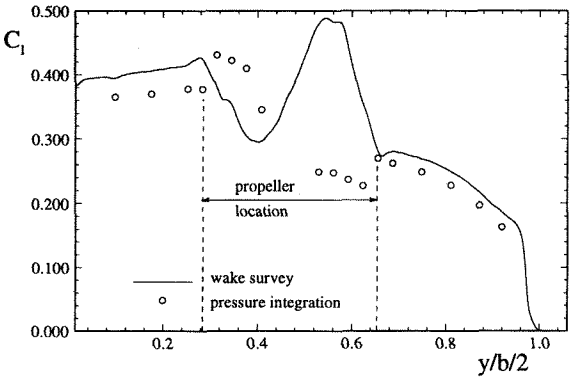

(b)

Figure 28: Comparison of the lift distributions found from the integrated surface pressures and from the flow field survey method at $\alpha = 4°$. (a) prop off, (b) prop on

the uninstalled propeller with a numerical code indicated that the changes in C_n-values in the slipstream indeed provide a reasonable representation of the normal force acting on the propeller. The increased loading at the downgoing blade is clearly visible as the peak in the local lift coefficient becomes higher than the values at the inboard side. From these figures it is reasonable to conclude that optimization of the wing alone with prescribed propeller input data, as suggested by Kroo [1], Miranda [2] and Veldhuis [6] should be replaced by an optimization of the complete propeller/wing combination in which all the iteraction effects are integrated.

Comparison with balance measurements The final results of the wake surveys are compared with the balance measurements in fig. 30 and 31. If we look at the effect of the propeller on the separate contributions of induced drag and profile drag we see that mainly the profile drag component is influenced as a result of the strong positive P_t-effect. The results of the calculations

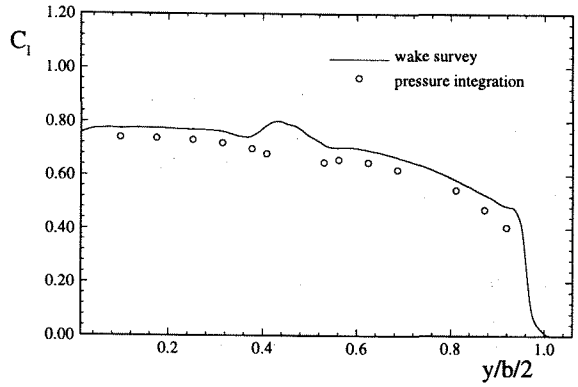

(a)

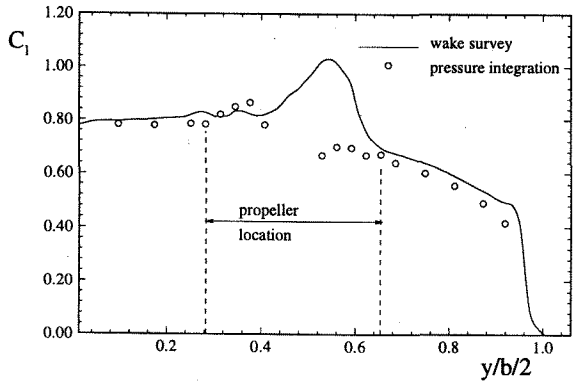

(b)

Figure 29: Comparison of the lift distributions found from the integrated surface pressures and from the flow field survey method at $\alpha = 10°$. (a) prop off, (b) prop on

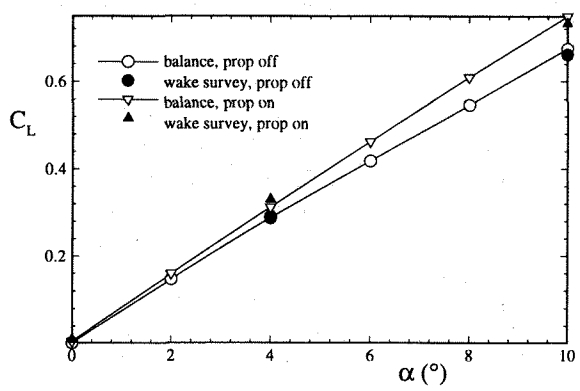

Figure 30: The overall lift coefficients found from external balance measurements and wake surveys

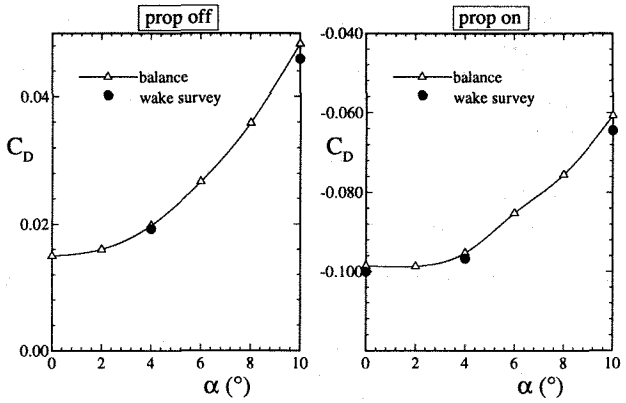

Figure 31: The overall drag coefficients found from external balance measurements and wake surveys

for $\alpha = 4°$ and $\alpha = 10°$ are presented in table . It is clear that the drag found in the case of a running propeller includes the thrust component and therefore becomes negative (fig. 31). From table it can be concluded that the favourable effect of the propeller, a negative $\Delta(C_{D_p})_{prop}$, becomes slightly less (about 14 counts) when the angle of attack is increased from 4° to 10°. It is however impossible to determine whether this is caused by a change of the wing profile drag or by a change in the slipstream characteristics due to angle of attack. Separate measurement of the propeller thrust with an internal balance will be necessary to draw conclusions in this respect. Although the flow field surveys produce a drag coefficient that is slightly smaller than the drag from the external balance measurements the agreement between the two techniques is quite good. The comparison of the overall lift coefficients, as presented in fig. 30, is even better. The agreement is better for the prop-off case (maximum difference of 2%) than for the prop-on case (maximum difference of 5%). No convenient explanation for this phenomenon is available at this moment.

Conclusions and recommendations

The following conclusions can be drawn from the experimental investigations:

- It is clear that significant improvements in aerodynamic efficiency may be obtained for optimised propeller positioning with reference to the wing. As was shown a high position of the propeller results in improved lift/drag behaviour. Particular reference is made to the possibility of performance increment using propellers with some degree of tilt down angle. For a practical use of negative propeller incidence angles however it should be noted that changes in thrust line orientation can produce significant changes in flow field uniformity and thus the propeller performance and the blade stress levels. This might also affect the overall noise production. In this field further analysis is needed taking

Table 2: Propeller influence on wing lift and drag

	α	4°	10°
C_{D_p}	prop on	-0.10609	-0.09411
	prop off	+0.01600	+0.02661
	$\Delta(C_{D_p})_{prop}$	**-0.12209**	**-0.12072**
C_{D_v}	prop on	+0.00717	+0.02774
	prop off	+0.00324	+0.01935
	$\Delta(C_{D_v})_{prop}$	**+0.00393**	**+0.00839**
C_D	prop on	-0.09893	-0.06637
	prop off	+0.01924	+0.04596
	$\Delta(C_D)_{prop}$	**-0.11817**	**-0.11233**
C_L	prop on	+0.3302	+0.7328
	prop off	+0.2917	+0.6618
	$\Delta(C_L)_{prop}$	**+0.0385**	**+0.0710**

into account all beneficial and detrimental effects to define optimum propeller/wing configurations.

- The efficiency of systems with up-inboard rotation exceeds that of systems with up-outboard rotation especially when the propeller is positioned at a small negative angle of attack. Consequently, serious investigation of the practical implementation of two up-inboard rotating propellers is recommended.
- The maximum performance increment occurred with the propeller positioned in an "over-the-wing" fashion. Since in general the aircraft longitudinal stability is benefits from an thrust line positioned above the c.g. of the aircraft no serious control problems for over the wing propeller aircraft should be expected. Thus the benefits of a over the wing propeller position combined with a propeller tilt down angle should be further analysed.
- Flow field surveys with a 5 hole probe behind the propeller/wing configuration with a fine grid spacing reveals valuable information on the structure of the slipstream and the lift and drag characteristics of the complete configuration.

The results might be used as a reference database to get a better understanding of the interaction between propellers and wings.

Acknowledgements

The author wishes to thank I. Philipsen, G.W. van Es, D.W.E Rentema and R. Esveldt for their thesis work, part of which is presented in this paper.

References

[1] Kroo, I. : "Propeller-measurements interaction for minimum induced loss", J. of Aircraft, Vol. 23, No. 7, july 1986, p. 561-565

[2] Miranda, L.R. and Brennan, J.E. : "Aerodynamic effects of wingtip-mounted propellers and turbines", AIAA 86-1802, 1986

[3] Witkowski, D.P. Lee,A.K.H. and Sullivan, J.P. : "Aerodynamic interaction between propellers and wings", AIAA paper No. 88-0665, AIAA 26th Aerospace Science Meeting, jan. 11-14, 1988,Reno, Nevada

[4] Veldhuis, L.L.M. : "Capabilities for testing 3D propeller powered windtunnel models at the Low Speed Laboratory of Delft University of Technology", Internal Rep ort LSW 92-8, 1992, Fac. of Aerospace Engineering, Delft University of Technology.

[5] Brune, G.W. and Bogataj, P.W., "Induced drag of a simple wing from wake measurements", AIAA-90-1934, 1990

[6] Veldhuis, L.L.M. : "Optimization of tractor propeller/wing configurations", Journal of Aerspace engineering, Part G, vol. 209, Proceedings of the Institute of Mechanical Engineers, june 1994

[7] Takallu, M.A. and Gentry G.L. : "Aerodynamic Characteristics of a propeller powered high lift semi-span wing", AIAA 92-0388

[8] Aljabri, A.S and Hughes, A.C. : "Wind tunnel investgation of the interaction of propeller slipstream with nacelle/wing/flap/combinations", AGARD FDP, Aerodynamics and Acoustics of propellers, AGARD DCP 366, paper nr. 21, Toronto, oct 1984

[9] Samuelsson, I. : "Low speed windtunnel investigation of propeller slistream aerodynamic effects on different nacelle/wing combinations", ICAS-88-4.11.1, 1988

[10] Williams, L.J. , Johnson, J.L. and Yipt, L.P. : "Some aerodynamic considerations for advanced aircraft configurations", AIAA paper 84-2508

[11] Leeuw, A. de : "Induced drag ; theory, measurements and calculations", Thesis Report, Delft University of Technology, 1993

[12] Rentema, D.W.E. : "Drag and lift calculations based on wake surveys of a propeller-wing combination at several angles of attack", Thesis Report, Delft University of Technology, 1994

[13] Krämer, E., Hertel, J. and Wagner, S. : "Euler procedure calculation of the steady rotor flow with emphasis on wake evolution", AIAA-90-3002-CP, 1990

[14] Betz, A. : "Ein verfahren zur direkten Ermittlung des Profielwoderstandes" Zeitschrift für Flugtechnik und Motorschiffahrt", Vol. 16, p.42, 1925

[15] Maskell, E.C. : "Progress towards a method for the measurement of components of the drag of a wing of finite span", RAE TR-72232, jan. 1973

[16] Wu, J.C. ,Hackett, J.E. and Lilley, D.E. : "A generalized wake-integral approach for drag determination in three-dimensional flows", AIAA 79-0279, 17th Aerospace Science meeting, New Orleans, La., jan. 1979

[17] Johnson, J.L. and White, E.R. : "Exploratory low speed wind-tunnel investigation of advanced commuter configurations including an over the wing propeller design", AIAA-83-2531, 1983

[18] Cooper, R.K. McCann, W.J. and Chapleo, A.Q. : "Over wing propeller aerodynamics", ICAS-92-3.2.2, p. 266, 1992

[19] Miley, C.S. : "Wing laminar boundary layer in the presence of a propeller slipstream", J. of Aircraft, Vol. 25, No. 7, p.606, 1987